

Higher Order Recurrent Space-Time Transformer for Video Action Prediction

Tsung-Ming Tai¹, Giuseppe Fiameni¹, Cheng-Kuang Lee¹, Oswald Lanz²

¹ NVIDIA AI Technology Center

² Fondazione Bruno Kessler

ntai@nvidia.com, gfiameni@nvidia.com, cklee@nvidia.com, lanz@fbk.eu

Abstract

Endowing visual agents with predictive capability is a key step towards video intelligence at scale. The predominant modeling paradigm for this is sequence learning, mostly implemented through LSTMs. Feed-forward Transformer architectures have replaced recurrent model designs in ML applications of language processing and also partly in computer vision. In this paper we investigate on the competitiveness of Transformer-style architectures for video predictive tasks. To do so we propose HORST, a novel higher order recurrent layer design whose core element is a spatial-temporal decomposition of self-attention for video. HORST achieves state of the art competitive performance on Something-Something early action recognition and EPIC-Kitchens action anticipation, showing evidence of predictive capability that we attribute to our recurrent higher order design of self-attention.

Introduction

Recognizing human actions from videos is a widely studied problem in computer vision. Most work has addressed action recognition as a video clip classification problem, lately almost exclusively with deep learning approaches, and a steady progress has pushed the limits of spatio-temporal feature learning from video. An underlying assumption in action recognition as clip classification is that of complete and synchronous observation, that is, the action to be recognized is immediately accessible and entirely represented in the clip. Such completeness assumption no longer holds with action prediction tasks, which is to forecast the future from observations of the past. In practice observations may be streamed and elaborated progressively to perform and revise future prediction continuously over time. These are requirements shared among many real world applications of video based prediction, e.g. in human-robot collaboration, real-time video surveillance, and autonomous driving.

We illustrate the problem setting of early action recognition and action anticipation, which are the two major video action prediction tasks, in Figure 1. As opposed to recognition, both require prediction of action labels beyond the extent of the observed video sub-clip. In early recognition, the target label is global and the action is already represented, even if not to its full extent, as a signal in the sub-clip. In anticipation, the target action only stays in causal relation to the signal in the sub-clip, but is not directly observable in it.

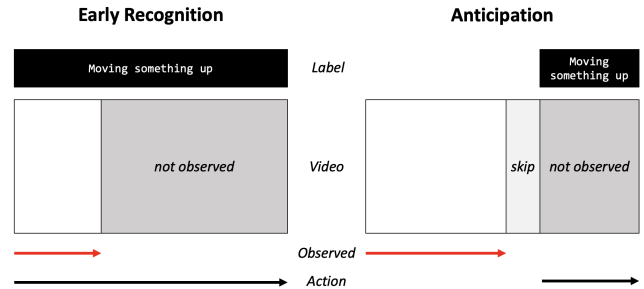


Figure 1: Early Recognition vs Anticipation. In early recognition the action can be partially observed, in anticipation it can only be inferred as a consequence of the observed.

It must be forecast as one possible consequence of the observed. While a clip classification design could be deployed for prediction, such an approach would not take advantage of these peculiar challenges that are not necessarily relevant for recognition. The problem to solve is different.

A standard modeling framework for anticipation and early recognition is recursive sequence prediction (Su et al. 2020; Furnari and Farinella 2020; Qi et al. 2021), where video frames are consumed in sequence to progressively update a representation of the relevant video content. Recent work has expanded upon LSTM or GRU design to realize models capable of capturing higher order correlations across time (Su et al. 2020), that fork parallel models at each iteration to simultaneously update a representation of the past while predicting the future with an encoder-decoder approach (Furnari and Farinella 2020), and revise intermediate representations through a dynamic re-weighting mechanism in a self-regulated learning framework (Qi et al. 2021). The shared objective of these works is to mitigate performance degradation due to accumulation of anticipation error. Some works furthermore attempt to tame the uncertainty induced by longer anticipation time through predicting multiple futures (Farha and Gall 2019) and by enforcing bidirectional predictions through cycle consistency (Farha et al. 2020).

In this paper we explore the design and effective learning of space-time transformers for predictive tasks such as early recognition and anticipation. Transformers have replaced recurrent models in ML applications of language

processing and also partly in computer vision. Latest work demonstrates that convolution-free, pure transformer architectures can compete with video CNNs on action classification (Bertasius, Wang, and Torresani 2021; Arnab et al. 2021). Timely enough, in this paper we investigate whether they can replace LSTMs on video predictive tasks, where LSTMs are still the common modeling paradigm of best performing methods. To verify this, we propose a novel higher order recurrent layer whose core element is a spatial-temporal decomposition of self-attention for video. It is higher order as it maintains a state queue in the attention mechanism to keep track of previously recorded information. It is recurrent in the way the queue is updated at each time step. Our layer is lightweight and has a transparent design, and achieves state of the art competitive performance when deployed for early action recognition and anticipation.

Related Work

Action Recognition. Classic approaches extract hand-crafted features from video and train a classifier on these to solve the task (Laptev 2005; Wang et al. 2013). Modern approaches blend feature extraction and classification into modular, end-to-end trainable neural architectures. Building on the success of 2D CNNs for image recognition, early approaches use temporal pooling of frame-level features to process video as a set of images (Wang et al. 2016; Girdhar et al. 2017) or use two-stream architectures to fuse frame features with features extracted from flow (Simonyan and Zisserman 2014; Feichtenhofer, Pinz, and Zisserman 2016). 3D CNNs process videos in space-time by expanding 2D kernels along the temporal dimension (Tran et al. 2015; Carreira and Zisserman 2017; Feichtenhofer 2020), requiring more parameters and compute. Learning spatio-temporal features with less is a shared objective of many recent works. These include decomposing 3D convolutions into 2D spatial followed by 1D temporal (Tran et al. 2018), replacing 1D with time shifts (Lin, Gan, and Han 2019) or gating (Sudhakaran, Escalera, and Lanz 2020), split channel dimensions using group convolutions (Tran et al. 2019), modeling interactions between separated dimensions (Li et al. 2020), and through adaptive fusion (Meng et al. 2021). Sequence learning models based on LSTM have been augmented with attention (Li et al. 2018; Girdhar and Ramanan 2017; Sudhakaran, Escalera, and Lanz 2019). Transformer inspired attention layers have been introduced in video CNNs (Girdhar et al. 2019; Wang et al. 2018; Chen et al. 2018), and recent studies show that pure self-attention based, convolution-free architectures can compete in action recognition (Bertasius, Wang, and Torresani 2021; Arnab et al. 2021).

Early Action Recognition. Works often expand upon action recognition architectures. Using a classifier trained on sub-clips is utilized as a baseline, which is valid in early recognition since the target action is already observed in the sub-clip. Given the nature of the problem that is to predict from an initial part of a frame sequence, a most intuitive framework can be that of recurrent models such as LSTMs. LSTM architectures can be trained under the assumption that recognition confidence should be non-decreasing as the

model observes more of the action by introducing a ranking loss (Ma, Sigal, and Sclaroff 2016). Following a same assumption, a multi-stage LSTM architecture integrating context-aware and action-aware is trained with a loss that encourages to make correct predictions as early as possible in the input sequence (Akbarian et al. 2017). Sequential context can be leveraged to reconstruct missing information in the features extracted from partial video by learning from fully observed action videos (Kong, Tao, and Fu 2017). LSTMs are the building blocks of a two-stream feedback network where one stream processes the input and the other models the temporal relations to promote the representation of temporal dependencies (Geest and Tuytelaars 2018). Eidetic LSTM (Wang et al. 2019) introduces an attentive mechanism to memorize local appearance or short-term motion, and use it to improve predictive spatio-temporal feature learning. A higher order LSTM with convolutional gates uses multiple inputs from the past to update its internal state (Su et al. 2020). Using tensor train decomposition, their extension effectively dominates compute and parameter count to grow at most linearly in time and space.

Action Anticipation. Differently from early recognition, anticipation is to predict the action from observations before it actually starts. The problem has been studied in the context of third person vision but recently also with major efforts in robotic and egocentric, first person vision. Early work combines a Markov decision process model with ideas from control theory to forecast human trajectories using semantic scene context (Kitani et al. 2012). (Koppula and Saxena 2016) propose a CRF framework which integrates object affordances to inform about possible future actions. (Vondrick, Pirsiavash, and Torralba 2016) address action anticipation by training a CNN to regress representations of future frames from past ones in an unsupervised way. A encoder-decoder LSTM network is presented in (Gao, Yang, and Nevatia 2017) which takes multiple past representations as input and learns to anticipate a time series of future representations. (Farha, Richard, and Gall 2018) investigate the use of CNN and GRU to learn future video labels based on previously seen content. An anticipatory model is combined with an auxiliary model to reason about how actions and scene attributes may co-evolve over time (Miech et al. 2019). RU-LSTM (Furnari and Farinella 2019) is a learning architecture which processes RGB frame snippets, optical flow and object features using two LSTMs and modality attention to anticipate future actions. The two LSTMs behave like an encoder-decoder, where the first progressively summarizes the observed together with the second that unrolls over future predictions without observing. A self-regulated learning framework is presented in (Qi et al. 2021), that utilizes LSTMs to progressively re-weight previously observed content, and to rectify predicted intermediate representations. (Fernando and Herath 2021) distill the information of the future to the past representation by maximizing the correlation between past and future frames in the feature space for video action prediction.

Higher Order Recurrent Networks. Following the first order Markov chain assumption, RNNs can efficiently pro-

cess sequential inputs by learning a transition model of underlying dynamics. In practice, it is difficult to train RNNs to capture long-term dependency due to vanishing or exploding gradients (Bengio, Simard, and Frasconi 1994). To better capture long term dependencies, (Soltani and Jiang 2016) keep track of more past states in a higher order recurrent network. Further studies analyze different aggregation functions to recur on the set of past states (Yu et al. 2017). (Su et al. 2020) derive a tensor-train decomposition of higher order convolutional LSTMs for video predictive tasks.

Vision Transformers. Vision Transformer (ViT) (Dosovitskiy et al. 2020) can handle the input spatial dimension by splitting the inputs into 16x16 patches. However, taking full advantage of the additional temporal dimension in video is still challenging. (Bertasius, Wang, and Torresani 2021) explores different self-attention schemes to incorporate spatial and temporal information for video recognition. (Arnab et al. 2021) further factorizes the spatial-temporal structure by deploying separated multi-head attentions for each spatial and temporal dimension. (Girdhar and Grauman 2021) propose a vision transformer based architecture for future action prediction with causal attention design. A distinguishing element in our work is that we do not apply patching and flattening to the input; we process the input at its full spatial resolution without imposing any structure prior (grid). Our custom decomposition of self-attention is also tightly integrated with a recurrent design to update the representation for future prediction from a queue of past representations.

Preliminaries

Higher Order Recurrence. Conventional recurrent networks, where the output of step t only depends on its previous $t - 1$ state, follow a *first order* Markov assumption

$$h_t = g(x_t, h_{t-1}) \quad (1)$$

where g can be any arbitrary nonlinear function including LSTM and GRU, x_t is the current input and h_t, h_{t-1} are current and previous hidden state. Extending to *higher order* Markov assumption, where the output of step t depends on multiple historical states $t - 1$ to $t - S$ with S indicating the *order*, equation (1) can be reformulated as

$$h_t = g(x_t, \phi(h_{t-1:t-S})) \quad (2)$$

where ϕ is an aggregation function for a state queue $h_{t-1:t-S}$. Various aggregation functions have been proposed, such as linear (Soltani and Jiang 2016), polynomial (Yu et al. 2017), and tensor-train (Su et al. 2020).

Attention. The attention proposed in (Vaswani et al. 2017) takes as input query Q , key K , and value V . The outcome is obtained by evaluating the dot-product between Q and K , scaled by a softmax function, and multiplying it to V

$$\text{ATT}(Q, K, V) = \text{softmax}\left(\frac{Q^T K}{\sqrt{C}}\right)V \quad (3)$$

where C is a scaling factor. The attention was designed for vector inputs. It is parameter-free, and the learning capacity in transformers is with the linear embeddings that map a given layer input x to the three attention inputs Q, K, V .

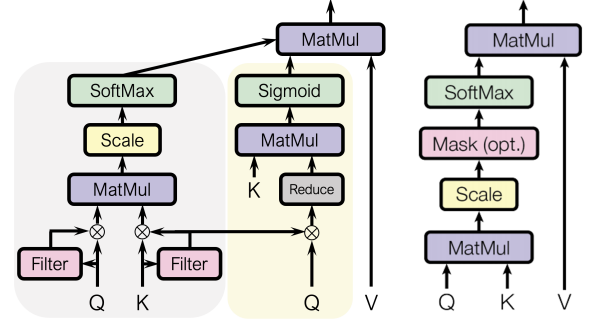


Figure 2: Left: Proposed Spatial-Temporal Attention. (Temporal branch is in grey area, and spatial branch is in yellow); Right: Attention in (Vaswani et al. 2017).

Method

Spatial-Temporal Attention

To exploit the effective information in spatial-temporal structure, we propose a light-weighted and computation-efficient attention, which integrates spatial and temporal operators from separated branches. Figure 2 compares the proposed spatial-temporal attention with the attention in (Vaswani et al. 2017). To define spatial and temporal branch operators, we introduce *spatial filter* maps f_K, f_Q for keys and query. Their role is attending the relevant spatial regions in keys and query. We use the following

$$f_{\mathcal{X}}(X) = \text{sigmoid}(\theta_{\mathcal{X}} * [X_{max}, X_{avg}] + b_{\mathcal{X}}) \quad (4)$$

where $*$ is convolution, X_{avg}, X_{max} are channel mean and max pooled, θ_K, θ_Q and b_K, b_Q are convolution kernels and biases, and sigmoid is to map to range [0:1]. We use f_K, f_Q as weight maps to filter keys and query for space-time attention.

Spatial branch: $S(Q, K)$ provides pixel-wise weight maps for spatial attention at each timestep. Weight maps are measured by the sigmoid of dot-product between keys and a global average pooling of filtered key-query comparisons

$$\begin{aligned} \hat{Q} &= \text{GlobalAveragePool}(f_K(K) \cdot Q) \\ S(Q, K) &= \text{sigmoid}(\hat{Q}^T K) \end{aligned} \quad (5)$$

where \cdot is element-wise multiplication.

Temporal branch: $T(Q, K)$ measures the importance weights in the temporal dimension. The weights are calculated by dot-product attention between self-filtered keys and query, followed by scaled softmax

$$\mathcal{T}(Q, K) = \text{softmax}\left(\frac{(f_Q(Q) \cdot Q)^T (f_K(K) \cdot K)}{\sqrt{C}}\right) \quad (6)$$

Spatial-temporal attention: Combining spatial and temporal branches, defined in (5) and (6), the proposed spatial-temporal decomposition of self-attention is

$$\text{STATT}(Q, K, V) = (S(Q, K) \otimes \mathcal{T}(Q, K)) \cdot V \quad (7)$$

where \otimes is cross-product. In this model, keys and query are utilized differently in spatial and temporal attention computation as they get pre-filtered by the learnable f_K, f_Q . Hence, our formulation of self-attention is not parameter-free.

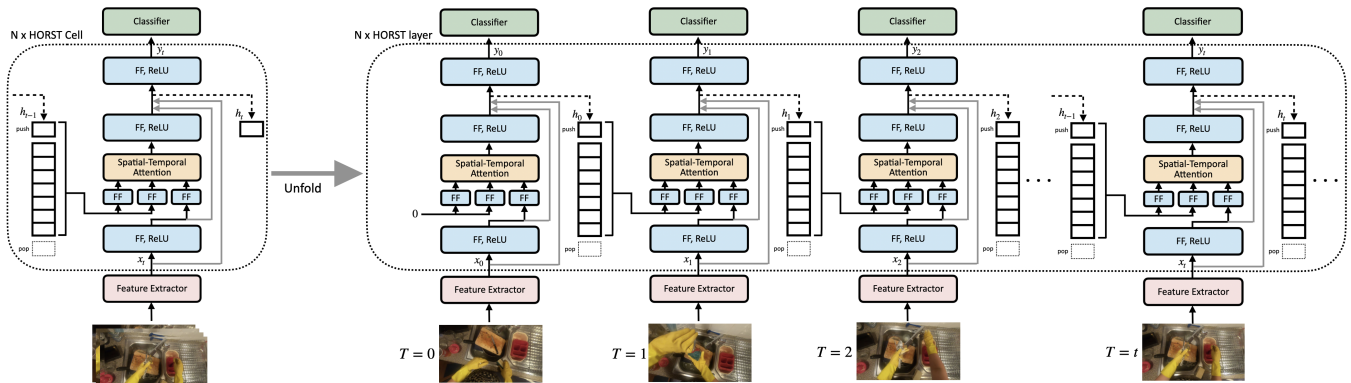


Figure 3: An overview of HORST for video prediction, in recurrent and unfold view.

Ops counts: Our spatial-temporal design requires $(6S + 1)CHW + 18(S + 1)HW$ ops, where S is the key-value sequence length. This is far less than $2S(HW)^2C$ of joint space-time attention (Bertasius, Wang, and Torresani 2021), and approximately twice the ops of full-temporal, $2SHWC$, while providing a more fine-grained attention design.

Higher Order Recurrent Space Time Transformer

Figure 3 shows an illustration of HORST architecture and its unfolding to process video inputs. All FF blocks are Conv-LayerNorm transformations. At each step t , we feed the video frame through a 2D-CNN backbone to obtain feature map x_t , and encode it with FF_x to obtain the intermediate representation e_t . We then project e_t to Q, K, V independently using FF_Q, FF_K, FF_V . The spatial-temporal attention output from (7) is then projected to h_t using FF_h . Layer output y_t is computed from h_t through a final FF_y informed by shortcuts x_t, e_t . The new state h_t is pushed to the queue and the oldest state h_{t-S} is released.

By instantiating ϕ in (2) with spatial-temporal attention from (7), a HORST layer can be formalized as

$$e_t = \text{ReLU}(FF_x(x_t)) \quad (8)$$

$$h_t = \text{ReLU}(FF_h(e_t + \text{STATT}(Q_t, K_{t-1:t-S}, V_{t-1:t-S})))$$

$$y_t = \text{ReLU}(FF_y(h_t + x_t))$$

with

$$Q_t = FF_Q(e_t) \quad (9)$$

$$K_{t-1:t-S} = FF_K([Q_{t-1:t-S}; h_{t-1:t-S}]) \quad (10)$$

$$V_{t-1:t-S} = FF_V([Q_{t-1:t-S}; h_{t-1:t-S}]) \quad (11)$$

where $[\cdot; \cdot]$ is concatenation.

HORST can be viewed as a transformer that processes sequence data in a recurrent manner with an internal memory queue managed by a first-in first-out policy. Having spatial-temporal attention as aggregation function ϕ in (2) makes HORST capable of accessing specific memory states while skipping others. Furthermore, our attention design is single-head. Multi-head tends to produce over-smoothed temporal weighting. We found empirically that the performance of HORST is stronger with single-head, considering the number of states is small. In our ablation study, we also show that

position encoding, which is widely adopted in transformer, is not needed in HORST given explicit recurrence. By attaching e_t in (8) to keys and values, the temporal position information is preserved.

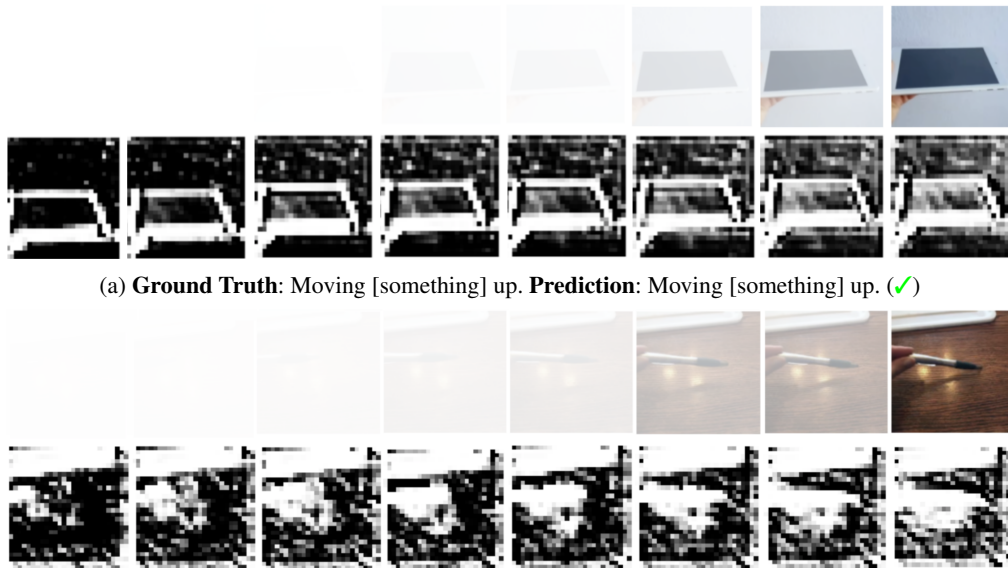
Experiments

Something-Something v2 (SSv2). SSv2 (Goyal et al. 2017) is a large collection of action video clips, with duration ranging from 2 to 6 seconds. We follow the data split scheme in (Wang et al. 2019) for early recognition, with a subset of 41 categories. There are a total 56769 video clips for training and 7503 for validation.

EPIC-Kitchens (EK55, EK100). EK55 (Damen et al. 2018) is a large scale egocentric video dataset, captured by 32 subjects in 32 kitchens. The action anticipation split is inherited from (Furnari and Farinella 2019) and amounts to 23492 action segments for training and 4979 for validation. Videos are categorized into 125 verbs and 352 nouns. All unique verb-noun pairs define 2513 action categories. EK100 (Damen et al. 2020) extends EK55 from 55 to 100 hours of video. EK100 considers 97 verbs and 300 nouns. Unique verb-noun pairs define 3087 action categories.

Implementation Details

Architecture. In early recognition on SSv2 dataset, two 3x3 convolution layers with 128 filters and stride 2 are stacked as backbone extractor, which shrinks the inputs from 224x224 to 56x56. Four HORST layers, with strides [1, 1, 2, 2], take the feature maps from backbone and produce 14x14 outputs. A classifier then transforms the HORST outputs into the target action predictions. In anticipation with EK55 and EK100 datasets, we use the pretrained BN-Inception model of (Furnari and Farinella 2019) as backbone. All input frames are resized to 256x454. The feature maps before the global average pooling in BN-Inception are extracted and fed through two HORST layers followed by a classifier forming the noun, verb, and action predictions. We also experiment with a task specific classifier design, where we adopt the unrolling LSTM from (Furnari and Farinella 2019). The unrolling classifier unfolds the final HORST output over the unobserved interval with an LSTM, till the mo-



(a) **Ground Truth:** Moving [something] up. **Prediction:** Moving [something] up. (✓)

(b) **Ground Truth:** Putting [something] on a flat surface without letting it roll. **Prediction:** Putting [something] on a surface. (✗)

Figure 4: Visualization samples on SSv2: we show input frames weighted by temporal attention and spatial attention maps from the final $S = 8$ timesteps leading to the prediction. Captions reveal ground-truth annotation and top-1 prediction.

ment where the action is expected to start, and then computes the predictions.

Training. We adopt RandAugment (Cubuk et al. 2020) in all experiments. We use AdaBelief (Zhuang et al. 2020) in combination with look-ahead optimizer (Zhang et al. 2019). Weight decay is set to 0.001. Learning rate is initially set to 0.002 and cosine annealed to 0 on the final 25% of epochs. The total training epochs is set to 50. We use $4 \times$ NVIDIA V100 32GB GPUs for training. Batch size is set to 8 for early recognition and 32 for anticipation.

Early Action Recognition

Sampling. We conduct early recognition on SSv2 dataset, when only the initial 25% or 50% of total frames are observed. Inputs are resized to 224×224 and all frames (24 fps) are used for prediction. Each sample is variable length.

Quantitative Results. Table 1 shows the top-1 accuracy compared with state-of-the-art methods in both 25% and 50% early recognition settings. All the recurrent-based methods outperform the 3D-CNN baseline. Conv-TT-LSTM is a 3-order ConvLSTM model with tensor-train decomposition. We reproduced Conv-TT-LSTM in our training protocol (e.g., augmentations, optimizer, and learning rate scheduling) resulting in significant improvements. HORST further achieves state-of-the-art performance by a large margin on both 25% and 50% settings, with +4.9% and +5.5% higher top-1 action accuracy than Conv-TT-LSTM.

Visualization Analysis. Figure 4 visualizes temporal (transparency on input frames) and spatial attention (second row) for two samples from the SSv2 validation set. Figure 4a is a sample with the ground truth Moving [something]

Table 1: SSv2 25% and 50% early action recognition results. † indicates reproduction by us using our training protocol.

Methods	Top-1 Accuracy(%)	
	25% frames	50% frames
3D-CNN	13.3	20.7
E3D-LSTM (Wang et al. 2019)	14.6	22.7
ConvLSTM	15.5	22.0
Conv-TT-LSTM (Su et al. 2020)	19.5	30.1
Conv-TT-LSTM†	29.3	42.3
HORST (Ours)	33.9	47.8

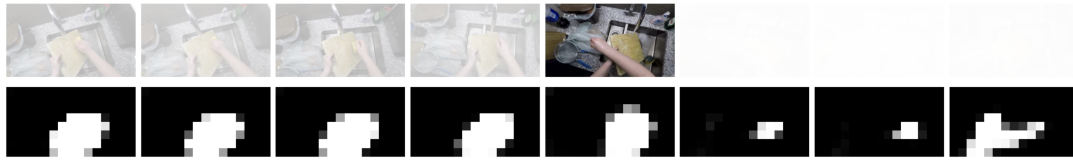
up. Spatial attention captures the border of the object whose vertical translation is clearly associated to the target action. Temporal attention focuses on the few recent states due to the steady movement of the sample. Figure 4b is an example with incorrect prediction. Without observing the subsequent frames, the model can hardly decide whether the object will be rolling or not. It is worth noting that in this sample, spatial-temporal attention produces the highest temporal weights when the object touched the surface, which is an important event for reasonable prediction.

Ablation Study

Ablations are all performed on SSv2 25% early recognition.

Spatial-Temporal Attention. We compare different attention variants in Table 2. Temporal only attention is with the constant $\mathcal{S}(Q, K) = 1$ instead of (5). Spatial only attention is with the constant $\mathcal{T}(Q, K) = \frac{1}{S}$ instead of (6). Spatial-temporal is our proposed attention using (6) and (5).

The performance differences with temporal only and spa-



(a) Ground Truth: Wash Board; Top-5 Predictions: Wash Board, Put-Down Board, Turn-Off Tap, Put-Down Sponge, Stir Pan.



(b) Ground Truth: Throw Onion; Top-5 Predictions: Open Door, Throw Skin, Take Onion, Take Skin, Take-Off Skin.

Figure 5: Visualization samples on EK55: we show input frames weighted by temporal attention and spatial attention maps from the final $S = 8$ timesteps leading to the predictions. Captions reveal ground-truth annotation and top-5 predictions.

Table 2: Ablation on attention design

Attention	Top-1 Accuracy (%)
$4 \times$ Temporal only	32.7
$4 \times$ Spatial only	31.2
$4 \times$ Spatial-Temporal	33.9
$2 \times$ Joint Space-Time	30.4
$2 \times$ Spatial-Temporal	32.2

Table 3: Impact of model order

Order	Top-1 Accuracy (%)
$S = 1$	30.7
$S = 3$	31.2
$S = 8$	33.9
$S = 12$	33.8
$S = 16$	32.7

Table 4: Ablation on choices for key and value

Key (K)	Value (V)	Acc (%)
$FF_K(e_{t-1:t-S})$	$FF_V(h_{t-1:t-S})$	30.6
$FF_K([e_{t-1:t-S}; h_{t-1:t-S}])$	$FF_V([e_{t-1:t-S}; h_{t-1:t-S}])$	33.9

tial only imply that both local spatial and temporal weighting using filtered state information is beneficial and best exploited when combined. We compare our spatial-temporal attention with joint space-time attention from (Bertasius, Wang, and Torresani 2021) using two layers¹. Ours achieves an absolute +1.8% gain over joint space-time with same number of layers. Using four HORST layers instead, gain raises to +3.5%.

Order. Table 3 compares model performance under different orders S . We observe the best accuracy when $S = 8, 12$. The drop in performance with $S = 16$ may relate to the

¹Because of heavy memory consumption, we cannot use four joint space-time attention layers with the same batch size. Lowering the batch size degrades its accuracy.

gradient instability issue reported in (Su et al. 2020)². Our higher order design shows significant improvement over the first order variant, achieving up to +3.2% higher accuracy.

Position Encoding. We compare two different choices for spatial-temporal attention inputs. Considering that spatial-temporal aggregates past states with different associated weights for each time step, first choice in the Table 4 causes key-value misaligned in time. Binding both key and value with e_t (which is directly encoded from the layer input x_t) provides the temporal position encoding to each time step in both K and V . Indeed, this leads to a +3.3% improvement.

Action Anticipation

Sampling. We conduct action anticipation on EK55 and EK100. We process 14 frames from each clip, sampled with fixed stride of 0.25s (4 fps). We use τ_a to indicate anticipation time.

Baselines. We compare all baselines in RGB only modality. We include Deep Multimodal Regressor (DMR), (Vondrick, Pirsivash, and Torralba 2016), TSN-based models MCE (Furnari, Battiato, and Maria Farinella 2018) and ATSN (Damen et al. 2018), deep network trained with top-k classifier (SVM-Top3/5) (Berrada, Zisserman, and Kumar 2018), Verb-Noun Marginal Cross Entropy (VNMCE) (Furnari, Battiato, and Maria Farinella 2018), and several LSTM variants, Encoder-Decoder LSTM (ED) (Gao, Yang, and Nevatia 2017), Feedback Network LSTM (FN) (Geest and Tuytelaars 2018), LSTM with Ranking Loss (RL) (Ma, Sigal, and Sclaroff 2016), and LSTM with Exponential Anticipation Loss (EL) (Jain et al. 2016). We also compare the state-of-the-art Rolling-Unrolling LSTM (RU) (Furnari and Farinella 2020), ImagineRNN by predicting future feature (Wu et al. 2020), and previous winners in EPIC-Kitchens anticipation challenge, ActionBanks in 2020 challenge (Sener, Singhania, and Yao 2020) and Anticipative Video Transformer (AVT) in 2021 (Girdhar and Grauman 2021).

²HORST can still enjoy higher order design with peak performance at $S = 8$, instead of $S = 3$ reported in prior works.

Table 5: EK55 Action Anticipation validation results using RGB. All methods on the table are based on the same BN-Inception with TSN backbone, from (Furnari and Farinella 2020). HORST-url applies unrolling on top of HORST.

Methods	Top-5 Accuracy (%) at different τ_a								Top-5 Acc. (%) @ 1s			Mean Top-5 Recall (%) @ 1s		
	2	1.75	1.5	1.25	1.0	0.75	0.5	0.25	Verb	Noun	Action	Verb	Noun	Action
DMR	-	-	-	-	16.86	-	-	-	73.66	29.99	16.86	24.50	20.89	03.23
ATSN	-	-	-	-	16.29	-	-	-	77.30	39.93	16.29	33.08	32.77	07.06
MCE	-	-	-	-	26.11	-	-	-	73.35	38.86	26.11	34.62	32.59	06.50
VN-CE	-	-	-	-	17.31	-	-	-	77.67	39.50	17.31	34.05	34.50	07.73
SVM-TOP3	-	-	-	-	25.42	-	-	-	72.70	28.41	25.42	41.90	34.69	05.32
SVM-TOP5	-	-	-	-	24.46	-	-	-	69.17	36.66	24.46	40.27	32.69	05.23
VNMCE+T3	-	-	-	-	25.95	-	-	-	74.05	39.18	25.95	40.17	34.15	05.57
VNMCE+T5	-	-	-	-	26.01	-	-	-	74.07	39.10	26.01	41.62	35.49	05.78
ED	21.53	22.22	23.20	24.78	25.75	26.69	27.66	29.74	75.46	42.96	25.75	41.77	42.59	10.97
FN	23.47	24.07	24.68	25.66	26.27	26.87	27.88	28.96	74.84	40.87	26.27	35.30	37.77	06.64
RL	25.95	26.49	27.15	28.48	29.61	30.81	31.86	32.84	76.79	44.53	29.61	40.80	40.87	10.64
EL	24.68	25.68	26.41	27.35	28.56	30.27	31.50	33.55	75.66	43.72	28.56	38.70	40.32	08.62
RU-RGB	25.44	26.89	28.32	29.42	30.83	32.00	33.31	34.47	-	-	30.83	-	-	-
HORST	25.38	26.37	27.82	29.16	30.69	31.54	32.52	33.45	77.67	46.34	30.69	36.54	44.33	10.94
HORST-url	25.95	27.03	28.24	29.81	31.58	32.68	34.21	35.56	78.80	46.54	31.58	42.62	45.68	12.18

Table 6: EK55 Action Anticipation validation results using RGB with top-1 and top-5 action accuracy at $\tau_a = 1s$.

Method	Backbone	Pretrain	Top-1 (%)	Top-5 (%)
RU-RGB	BNInc	In1k	13.1	30.8
ActionBanks	BNInc	In1k	12.3	28.5
ImagineRNN	BNInc	In1k	13.7	31.6
AVT-h	BNInc	In1k	13.1	28.1
AVT-h	AVT-b	In21+1k	12.5	30.1
AVT-h	irCSN152	IG65M	14.4	31.7
HORST	BNInc	In1k	12.6	30.7
HORST-url	BNInc	In1k	12.8	31.6

Table 7: EK100 Action Anticipation validation results using RGB with mean top-5 recall (%) at 1s.

Method	Backbone	Pretrain	Verb	Noun	Action
RU-RGB	BNInc	In1k	27.5	29.0	13.3
AVT-h	BNInc	In1k	27.3	30.7	13.6
AVT-h	AVT-b	In21+1k	28.7	32.3	14.4
AVT-h	irCSN152	IG65M	25.5	28.1	12.8
HORST	BNInc	In1k	23.8	29.2	13.2
HORST-url	BNInc	In1k	24.5	30.0	13.2

Quantitative Results. Table 5 reports top-5 accuracy at different anticipation times τ_a , and presents top-5 accuracy and top-5 mean recall for each verb, noun and action at $\tau_a = 1s$. Without any task specific design, HORST obtains 30.69% top-5 action accuracy at $\tau_a = 1s$. By equipping it with an unrolling classifier initialized from spatial-temporal states, e_t and h_t in equation (8), top-5 accuracy boosts to 31.58%, which is +0.75% higher than state-of-the-art RULSTM. More comparisons on top-1 and top-5 accuracy are included in Table 6. Under the same BN-Inception backbone, HORST achieves competitive top-5 accuracy over previous competition winners (ActionBanks, AVT), and comes with +0.9% top-5 improvements when integrating the unrolling classifier. We observe lower top-1 scores, this may be due to cases where input observations are spanned over the previous action duration and could mislead the predictions by ir-

relevant frames with similar scenes or objects. Such overlapping causes distraction with negative impact on target action prediction, and the unrolling classifier may even amplify it. The same behavior is not found in early recognition.

Table 7 shows quantitative results on EK100 dataset. AVT with irCSN152 backbone does not perform well on EK100, but is the strongest configuration in EK55. In contrast, AVT with AVT-b backbone has the best performance on EK100 but not on EK55. Such discrepancy can be the recall is used in evaluation, which reflects the par class performance but is hardly captured in top-1/5 accuracy measurements. HORST(-url) achieves the overall balanced performance on both EK55 and EK100. Although lower verb recall is observed, the noun and action are at the top level. We marked this difference as the direction to further develop upon our spatial-temporal attention design in future work.

Visualization Analysis. Figure 5a shows an example with correct prediction on *Wash Board*. We can see the model only referencing the necessary states, which demonstrates that temporal attention is capable of skipping some specific frames. Spatial attention spots the hand movement successfully. Figure 5b reveals a challenging example labeled *Throw Onion*. The model struggles between *onion* and *skin* in top-5 noun predictions, by failing to locate the chopped onions on the cutting board shown in the very first two frames in the figure. Instead, the human hand and the onion skins are spotted, yielding the inaccurate, but plausible, top-5 predictions.

Conclusion

We have presented HORST, a Transformer-style architecture for video action prediction. Our model is simple, lightweight, and has a transparent design. Its spatial-temporal decomposition of self-attention exposes visual explanations of model behaviors. HORST matches state-of-the-art performance on anticipation, and achieves superior performance on early recognition by a larger margin.

References

- Akbarian, M. S. A.; Saleh, F.; Salzmann, M.; Fernando, B.; Petersson, L.; and Andersson, L. 2017. Encouraging LSTMs to Anticipate Actions Very Early. In *ICCV*, 280–289.
- Arnab, A.; Dehghani, M.; Heigold, G.; Sun, C.; Lucic, M.; and Schmid, C. 2021. ViViT: A Video Vision Transformer. *CoRR*, abs/2103.15691.
- Bengio, Y.; Simard, P.; and Frasconi, P. 1994. Learning long-term dependencies with gradient descent is difficult. *IEEE transactions on neural networks*, 5(2): 157–166.
- Berrada, L.; Zisserman, A.; and Kumar, M. P. 2018. Smooth Loss Functions for Deep Top-k Classification. In *ICLR*.
- Bertasius, G.; Wang, H.; and Torresani, L. 2021. Is Space-Time Attention All You Need for Video Understanding? *CoRR*, abs/2102.05095.
- Carreira, J.; and Zisserman, A. 2017. Quo Vadis, Action Recognition? A New Model and the Kinetics Dataset. In *CVPR*, 4724–4733.
- Chen, Y.; Kalantidis, Y.; Li, J.; Yan, S.; and Feng, J. 2018. A²-Nets: Double Attention Networks. In *NeurIPS*, 350–359.
- Cubuk, E. D.; Zoph, B.; Shlens, J.; and Le, Q. V. 2020. Randaugment: Practical automated data augmentation with a reduced search space. In *CVPR Workshops*, 702–703.
- Damen, D.; Doughty, H.; Farinella, G. M.; ; Furnari, A.; Ma, J.; Kazakos, E.; Moltisanti, D.; Munro, J.; Perrett, T.; Price, W.; and Wray, M. 2020. Rescaling Egocentric Vision. *CoRR*, abs/2006.13256.
- Damen, D.; Doughty, H.; Farinella, G. M.; Fidler, S.; Furnari, A.; Kazakos, E.; Moltisanti, D.; Munro, J.; Perrett, T.; Price, W.; et al. 2018. Scaling egocentric vision: The epic-kitchens dataset. In *ECCV*, 720–736.
- Dosovitskiy, A.; Beyer, L.; Kolesnikov, A.; Weissenborn, D.; Zhai, X.; Unterthiner, T.; Dehghani, M.; Minderer, M.; Heigold, G.; Gelly, S.; et al. 2020. An image is worth 16x16 words: Transformers for image recognition at scale. *arXiv preprint arXiv:2010.11929*.
- Farha, Y. A.; and Gall, J. 2019. Uncertainty-Aware Anticipation of Activities. In *ICCV Workshops*, 1197–1204.
- Farha, Y. A.; Ke, Q.; Schiele, B.; and Gall, J. 2020. Long-Term Anticipation of Activities with Cycle Consistency. *CoRR*, abs/2009.01142.
- Farha, Y. A.; Richard, A.; and Gall, J. 2018. When Will You Do What? - Anticipating Temporal Occurrences of Activities. In *CVPR*, 5343–5352.
- Feichtenhofer, C. 2020. X3D: Expanding Architectures for Efficient Video Recognition. In *CVPR*, 200–210.
- Feichtenhofer, C.; Pinz, A.; and Zisserman, A. 2016. Convolutional Two-Stream Network Fusion for Video Action Recognition. In *CVPR*, 1933–1941.
- Fernando, B.; and Herath, S. 2021. Anticipating human actions by correlating past with the future with Jaccard similarity measures. In *Proceedings of the IEEE/CVF Conference on Computer Vision and Pattern Recognition*, 13224–13233.
- Furnari, A.; Battiato, S.; and Maria Farinella, G. 2018. Leveraging uncertainty to rethink loss functions and evaluation measures for egocentric action anticipation. In *ECCV Workshops*.
- Furnari, A.; and Farinella, G. M. 2019. What Would You Expect? Anticipating Egocentric Actions With Rolling-Unrolling LSTMs and Modality Attention. In *ICCV*, 6251–6260.
- Furnari, A.; and Farinella, G. M. 2020. Rolling-Unrolling LSTMs for Action Anticipation from First-Person Video. *IEEE Transactions on Pattern Analysis and Machine Intelligence*.
- Gao, J.; Yang, Z.; and Nevatia, R. 2017. RED: Reinforced Encoder-Decoder Networks for Action Anticipation. In *BMVC*.
- Geest, R. D.; and Tuytelaars, T. 2018. Modeling Temporal Structure with LSTM for Online Action Detection. In *WACV*, 1549–1557.
- Girdhar, R.; Carreira, J.; Doersch, C.; and Zisserman, A. 2019. Video Action Transformer Network. In *CVPR*, 244–253.
- Girdhar, R.; and Grauman, K. 2021. Anticipative Video Transformer. *arXiv preprint arXiv:2106.02036*.
- Girdhar, R.; and Ramanan, D. 2017. Attentional Pooling for Action Recognition. In *NeurIPS*, 34–45.
- Girdhar, R.; Ramanan, D.; Gupta, A.; Sivic, J.; and Russell, B. C. 2017. ActionVLAD: Learning Spatio-Temporal Aggregation for Action Classification. In *CVPR*, 3165–3174.
- Goyal, R.; Kahou, S. E.; Michalski, V.; Materzynska, J.; Westphal, S.; Kim, H.; Haenel, V.; Fründ, I.; Yianilos, P.; Mueller-Freitag, M.; Hoppe, F.; Thureau, C.; Bax, I.; and Memisevic, R. 2017. The “Something Something” Video Database for Learning and Evaluating Visual Common Sense. In *ICCV*, 5843–5851.
- Jain, A.; Singh, A.; Koppula, H. S.; Soh, S.; and Saxena, A. 2016. Recurrent Neural Networks for driver activity anticipation via sensory-fusion architecture. In *ICRA*, 3118–3125.
- Kitani, K. M.; Ziebart, B. D.; Bagnell, J. A.; and Hebert, M. 2012. Activity Forecasting. In *ECCV*, 201–214.
- Kong, Y.; Tao, Z.; and Fu, Y. 2017. Deep Sequential Context Networks for Action Prediction. In *CVPR*, 3662–3670.
- Koppula, H. S.; and Saxena, A. 2016. Anticipating Human Activities Using Object Affordances for Reactive Robotic Response. *IEEE Transactions on Pattern Analysis and Machine Intelligence*, 38(1): 14–29.
- Laptev, I. 2005. On Space-Time Interest Points. *International Journal of Computer Vision*, 64(2-3): 107–123.
- Li, Y.; Ji, B.; Shi, X.; Zhang, J.; Kang, B.; and Wang, L. 2020. TEA: Temporal Excitation and Aggregation for Action Recognition. In *CVPR*, 906–915.
- Li, Z.; Gavriluyk, K.; Gavves, E.; Jain, M.; and Snoek, C. G. M. 2018. VideoLSTM convolves, attends and flows for action recognition. *Computer Vision and Image Understanding*, 166: 41–50.
- Lin, J.; Gan, C.; and Han, S. 2019. TSM: Temporal Shift Module for Efficient Video Understanding. In *ICCV*, 7082–7092.
- Ma, S.; Sigal, L.; and Sclaroff, S. 2016. Learning Activity Progression in LSTMs for Activity Detection and Early Detection. In *CVPR*, 1942–1950.
- Meng, Y.; Panda, R.; Lin, C.; Sattigeri, P.; Karlinsky, L.; Saenko, K.; Oliva, A.; and Feris, R. 2021. AdaFuse: Adaptive Temporal Fusion Network for Efficient Action Recognition. *CoRR*, abs/2102.05775.
- Miech, A.; Laptev, I.; Sivic, J.; Wang, H.; Torresani, L.; and Tran, D. 2019. Leveraging the Present to Anticipate the Future in Videos. In *CVPR Workshops*, 2915–2922.
- Qi, Z.; Wang, S.; Su, C.; Su, L.; Huang, Q.; and Tian, Q. 2021. Self-Regulated Learning for Egocentric Video Activity Anticipation. *IEEE Transactions on Pattern Analysis and Machine Intelligence*.
- Qi, Z.; Wang, S.; Su, C.; Su, L.; Huang, Q.; and Tian, Q. 2021. Self-Regulated Learning for Egocentric Video Activity Anticipation. *IEEE Transactions on Pattern Analysis and Machine Intelligence*.

Sener, F.; Singhania, D.; and Yao, A. 2020. Temporal aggregate representations for long-range video understanding. In *European Conference on Computer Vision*, 154–171. Springer.

Simonyan, K.; and Zisserman, A. 2014. Two-Stream Convolutional Networks for Action Recognition in Videos. In *NeurIPS*, 568–576.

Soltani, R.; and Jiang, H. 2016. Higher order recurrent neural networks. *arXiv preprint arXiv:1605.00064*.

Su, J.; Byeon, W.; Kossaifi, J.; Huang, F.; Kautz, J.; and Anandkumar, A. 2020. Convolutional Tensor-Train LSTM for Spatio-Temporal Learning. In *NeurIPS*.

Sudhakaran, S.; Escalera, S.; and Lanz, O. 2019. LSTA: Long Short-Term Attention for Egocentric Action Recognition. In *CVPR*, 9954–9963.

Sudhakaran, S.; Escalera, S.; and Lanz, O. 2020. Gate-Shift Networks for Video Action Recognition. In *CVPR*, 1099–1108.

Tran, D.; Bourdev, L. D.; Fergus, R.; Torresani, L.; and Paluri, M. 2015. Learning Spatiotemporal Features with 3D Convolutional Networks. In *ICCV*, 4489–4497.

Tran, D.; Wang, H.; Feiszli, M.; and Torresani, L. 2019. Video Classification With Channel-Separated Convolutional Networks. In *ICCV*, 5551–5560.

Tran, D.; Wang, H.; Torresani, L.; Ray, J.; LeCun, Y.; and Paluri, M. 2018. A Closer Look at Spatiotemporal Convolutions for Action Recognition. In *CVPR*, 6450–6459.

Vaswani, A.; Shazeer, N.; Parmar, N.; Uszkoreit, J.; Jones, L.; Gomez, A. N.; Kaiser, L.; and Polosukhin, I. 2017. Attention is All you Need. In *NeurIPS*, 5998–6008.

Vondrick, C.; Pirsaviash, H.; and Torralba, A. 2016. Anticipating Visual Representations from Unlabeled Video. In *CVPR*, 98–106.

Wang, H.; Kläser, A.; Schmid, C.; and Liu, C. 2013. Dense Trajectories and Motion Boundary Descriptors for Action Recognition. *International Journal of Computer Vision*, 103(1): 60–79.

Wang, L.; Xiong, Y.; Wang, Z.; Qiao, Y.; Lin, D.; Tang, X.; and Gool, L. V. 2016. Temporal Segment Networks: Towards Good Practices for Deep Action Recognition. In *ECCV*.

Wang, X.; Girshick, R. B.; Gupta, A.; and He, K. 2018. Non-Local Neural Networks. In *CVPR*, 7794–7803.

Wang, Y.; Jiang, L.; Yang, M.; Li, L.; Long, M.; and Fei-Fei, L. 2019. Eidetic 3D LSTM: A Model for Video Prediction and Beyond. In *ICLR*.

Wu, Y.; Zhu, L.; Wang, X.; Yang, Y.; and Wu, F. 2020. Learning to Anticipate Egocentric Actions by Imagination. *IEEE Transactions on Image Processing*, 30: 1143–1152.

Yu, R.; Zheng, S.; Anandkumar, A.; and Yue, Y. 2017. Long-term forecasting using tensor-train rnns. *Arxiv*.

Zhang, M.; Lucas, J.; Ba, J.; and Hinton, G. E. 2019. Lookahead Optimizer: k steps forward, 1 step back. In *NeurIPS*, volume 32.

Zhuang, J.; Tang, T.; Ding, Y.; Tatikonda, S. C.; Dvornik, N. C.; Papademetris, X.; and Duncan, J. S. 2020. AdaBelief Optimizer: Adapting Stepsizes by the Belief in Observed Gradients. In *NeurIPS*.

A Details on Classifier Designs

In the following, we use $\text{FC}(v)$ to denote a linear (fully-connected) transformation on vector v . The parameters of different FC’s are distinguished by their subscripts.

A.1 Early Action Recognition

For early action recognition on SSv2 dataset, only the single action label for each sample is available. We took global average pooling followed by a flatten operator to obtain a 1D vector of y_t (eq. (8) in the main paper), which is \overline{y}_t . The flattened 1D vector is then fed through a fully-connected layer, $\text{FC}(\overline{y}_t)$, to obtain the action logits. The cross-entropy loss is deployed to compare between the action logit and the ground-truth action label at the last timestep, in both 25% and 50% settings.

A.2 Anticipation

As above, we took global average pooling followed by a flatten operator to obtain a 1D vector of e_t as \overline{e}_t , and do the same on STATT_t and y_t as $\overline{\text{STATT}}_t$ and \overline{y}_t (see eq. (7)(8) for the variables). The anticipation classifier is computed by:

$$\chi_a = [\overline{e}_t; \overline{y}_t; \overline{\text{STATT}}_t] \quad (12)$$

$$\chi_v = \overline{\text{STATT}}_t \quad (13)$$

$$\chi_n = \overline{e}_t \quad (14)$$

and

$$\text{logit}_a = \text{FC}_a(\chi_a) \quad (15)$$

$$\text{logit}_v = \text{FC}_v(\chi_v + \text{FC}_{a2v}(\text{logit}_a)) \quad (16)$$

$$\text{logit}_n = \text{FC}_n(\chi_n + \text{FC}_{a2n}(\text{logit}_a)) \quad (17)$$

where the logit_a is also served as biases to logit_v and logit_n for explicitly building the relationship of action to the verb and noun, and also to back-prop the supervision signals more fluently.

The cross-entropy loss is used to compare between logits and ground-truth labels. The overall loss function is the summation over the individual loss of each action, verb, and noun, for every anticipation time.

A.3 Anticipation with Unrolling

HORST-url is shown in table 5-7 in the main paper with the unrolling classifier. The unrolling LSTM is performed on the final HORST outputs. The hidden and memory states of the unrolling LSTM are initialized by the \overline{e}_t and $\overline{\text{STATT}}_t$,

$$\xi_v = \text{ReLU}(\text{FC}_{\xi_v}(\overline{e}_t + \overline{\text{STATT}}_t)) \quad (18)$$

$$\xi_n = \text{ReLU}(\text{FC}_{\xi_n}(\overline{e}_t + \overline{\text{STATT}}_t)) \quad (19)$$

$$\text{feat} = \text{ReLU}(\text{FC}_{\text{feat}}([\xi_v; \xi_n])) \quad (20)$$

$$c_0^{url} = \text{FC}_c(\text{feat}) \quad (21)$$

$$h_0^{url} = \text{FC}_h(\text{feat}) \quad (22)$$

the states are unrolled T steps, where $T = \tau_a \times \text{fps}$, with the consistent input \overline{y}_t ,

$$(h_T^{url}, c_T^{url}) = \text{LSTMCell}(\overline{y}_t, (h_{T-1}^{url}, c_{T-1}^{url})) \quad (23)$$

We leverage the final unrolling output h_T^{url} for further logits calculation, with the following inputs:

$$\chi_a = h_T^{url} \quad (24)$$

$$\chi_v = \xi_v \quad (25)$$

$$\chi_n = \xi_n \quad (26)$$

Note that we supervise (verb, noun) on (16) and (17) with the inputs ξ_v and ξ_n to regularize the representation in the unrolling process.

B Training Time

For early recognition on SSv2 dataset, the model of four HORST layers with hidden states set to [128, 256, 512, 512] is deployed. The total training time is about 25 hours per run on 25% setting, this time is doubled in the 50% setting. For action anticipation on EK55 dataset, we train two HORST layers with the hidden state set to 1024 on top of frozen BN-Inception backbone, the training needs to take about 50 hours per run. We set hidden state to 512 on EK100 to keep roughly the same computation budgets. All are conducted on $4 \times \text{NVIDIA V-100 GPUs}$.

C Code

We present a PyTorch implementation of HORST layer in Figure 6. We also include code files of this implementation (`horst.py`), and of the classifiers described in Sec. A.2 (`cls-epic.py`) and Sec. A.3 (`cls-url-epic.py`). These codes were used to produce the results reported in the main paper. All the codes are released at <https://github.com/CorcovadoMing/HORST>

```

import torch
from torch import nn
import torch.nn.functional as F

class SpatialFilter(nn.Module):
    def __init__(self):
        super().__init__()
        self.f = nn.Sequential(nn.Conv2d(2, 1, 3, 1, 1), nn.Sigmoid())

    def forward(self, x):
        # x: (b, c, h, w)
        # Implementation of Eq. (4)
        avg_pool = x.mean(1, keepdim=True)
        max_pool = x.max(1, keepdim=True)[0]
        return self.f(torch.cat([avg_pool, max_pool], dim=1))

class STATT(nn.Module):
    def __init__(self, channels):
        super().__init__()
        self.sf_Q = SpatialFilter()
        self.sf_K = SpatialFilter()

    def forward(self, Q, K, V):
        # q: (1, b, c, h, w)
        # k: (s, b, c, h, w)
        # v: (s, b, c, h, w)

        f_Q = self.sf_Q(Q.reshape(Q.size(0)*Q.size(1), *Q.shape[2:])) \
            .reshape(*Q.shape[:2], 1, *Q.shape[3:])
        f_K = self.sf_K(K.reshape(K.size(0)*K.size(1), *K.shape[2:])) \
            .reshape(*K.shape[:2], 1, *K.shape[3:])

        # Spatial branch - Implementation of Eq. (5)
        f_KQ = (f_K * Q).mean([-1, -2]) # \hat{Q} in Eq. (5)
        S = torch.sigmoid(torch.einsum('sbc,sbcd->sbd', f_KQ, K.reshape(*K.shape[:3], -1)))
        S = S.reshape(*V.shape[:2], 1, *V.shape[-2:]).expand_as(V)
        V = V * S # Eq. (7) - spatial part

        # Temporal branch - Implementation of Eq. (6)
        Q = (Q * f_Q).reshape(*Q.shape[:2], -1)
        K = (K * f_K).reshape(*K.shape[:2], -1)
        T = torch.einsum('lbd,sbd->lsb', Q, K)
        T = F.softmax(T * (Q.size(-1) ** -0.5), dim=1)
        V = torch.einsum('lsb,sbchw->bchw', T, V) # Eq. (7) - temporal part
        return V

```

Figure 6: PyTorch implementation of our spatial-temporal decomposition of self-attention in HORST. It includes Eq. (4-7) of the main paper.